

Real-time seismic monitoring of Veterans Affairs hospital buildings

Hasan S. Ulusoy^{*a}, Erol Kalkan^b, and Krishna Banga^c

^a345 Middlefield Road MS 977, Menlo Park, CA 94025, USA

^bUnited States Geological Survey, Menlo Park, CA 94025, USA

^cDepartment of Veterans Affairs, Washington, DC, 20001, USA

ABSTRACT

This paper describes recent collaborative efforts made by the United States Geological Survey and Department of Veterans Affairs (VA) in real-time seismic monitoring of VA hospital buildings located in seismically active regions. The instrumentation in each building encompasses accelerometers deployed on all floors, a multi-channel recorder, and a server to analyze and archive the building's dynamic response in real-time. The server runs advanced structural health monitoring software, which consists of several data processing and analysis modules. Four different algorithms are implemented in four separate modules to compute shear-wave travel time, modal parameters, base shear force, and inter-story drift ratio from the measured vibration data from the instrumented building. The performance level and damage state of the building are estimated from the inter-story drift ratio and base-shear; the change in modal parameters and wave travel time is also used to detect and locate any possible damage zone(s) in the building. These algorithms are validated and verified using data from full-scale shake table tests. The information obtained from the real-time seismic monitoring system can be used to support timely decisions regarding the structural integrity of the VA hospital buildings immediately after an earthquake, and to help with inspections and necessary repairs and replacements.

Keywords: Seismic monitoring, instrumentation, earthquake, vibration data, damage detection and locating, system identification, structural health monitoring

1. INTRODUCTION

In 1971, an earthquake with magnitude of 6.6 hit San Fernando Valley in southern California, and resulted in collapse of several Olive View and San Fernando Department of Veterans Affairs (VA) hospital buildings. The VA hospital buildings had been built in 1925, before building codes were in effect. This catastrophe is a reminder that the integrity of the nation's hospital buildings is vital for the survival and functioning of the society in the aftermath of a catastrophic event. Following the 1971 earthquake, the VA's current Seismic Vulnerability Assessment Program was established to identify and strengthen hospital buildings that needed to be brought up to seismic safety standards. An important component of this program is to monitor earthquake shaking in hospital buildings. In collaboration with the VA, United States Geological Survey's National Strong Motion Project (NSMP) installed analog accelerographs in 65 VA medical buildings across the country immediately after the 1971 event. Later, in 2003, 45 of these instruments were upgraded to modern digital ones. In the last four years, VA buildings have been instrumented with dense arrays of seismic sensors to better understand their response to strong ground shaking. To date, the NSMP works closely with VA to monitor earthquake shaking in more than 80 VA medical buildings across the country. This effort helps the VA to better assess their building inventory and respond during future earthquakes.

The integrity of the nation's VA hospital buildings is critical for the survival and welfare of the society; this includes periodical assessment of their current conditions based on available information including measured data, and visual inspections and also evaluation of their safety after a damaging earthquake in order to support decisions regarding necessary repairs, replacements, and other maintenance and rehabilitation procedures. In this regard, vibration based structural health monitoring (SHM) and damage detection methods are viable tools to assess the structural integrity of hospital buildings in a quantitative manner.

SHM, regarded as an application of inverse problems¹ in structural dynamics, is the use of in-situ non-destructive sensing and analysis of system characteristics—in the time, frequency, or modal domains—for the purpose of detecting changes, which may indicate damage or degradation². The comprehensive review of the SHM and damage detection

* E-mail: hulusoy@usgs.gov; Ph: +1-650 329-4707

algorithms and techniques, which use changes in vibration characteristics, is provided by Doebling et al.³, Hohn et. al.⁴ and Catbas et al²¹. The techniques and algorithms developed for SHM and damage detection, based on the measured vibration data, significantly vary depending upon the intensity, frequency content and spatial distribution of measured data, the type of the structure under consideration, and the damage indicator (a parameter sensitive to damage in the structure). The selection of the damage indicator and the determination of its threshold values are of critical importance to the success of the detection algorithm in diagnosing the existence of the damage.

2. INSTRUMENTATION OF VA HOSPITAL BUILDINGS

The NSMP has recently completed new multi-channel instrumentation of 24 VA hospital buildings all across the United States, and such instrumentation of four more hospital buildings is in progress. Figure 1 shows the location of the 28 hospitals on a seismic hazard map of the U.S.

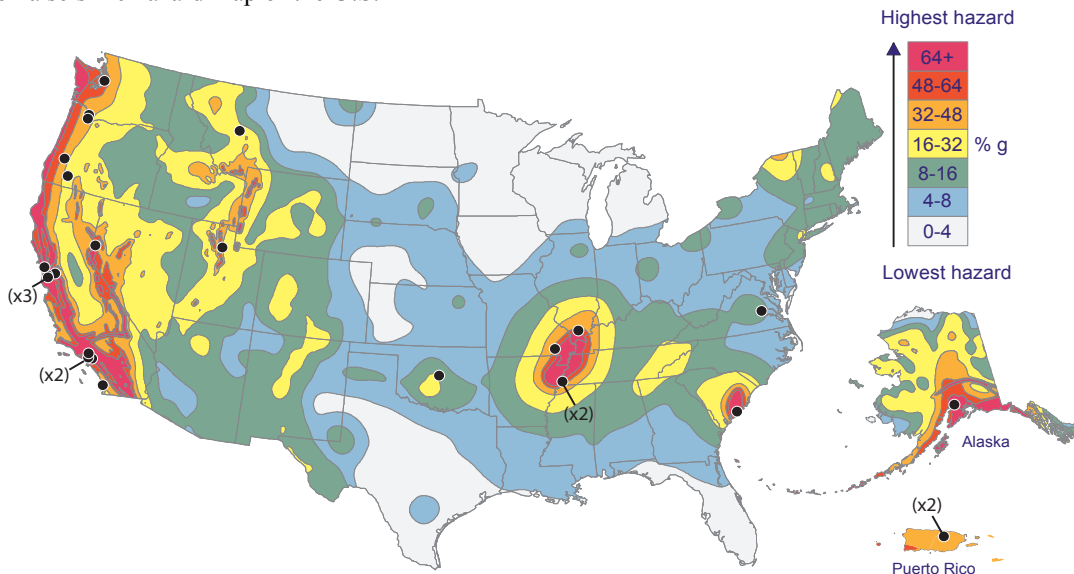


Figure 1. Seismic hazard map of the conterminous United States, Alaska, and Puerto Rico, showing the locations of 28 VA medical centers (black dots)—24 of these are already equipped with advanced earthquake monitoring systems, and the remainder will be by the end of 2013. Most of these hospital buildings are located in regions of high or very high seismic hazard. Colors on this map show the levels of horizontal shaking that have a 2% probability of exceedance in a 50-year period. Peak ground acceleration is expressed as a percentage of g. The seismic hazard map is available at <http://pubs.usgs.gov/fs/2008/3018/>.

The system designed for seismic monitoring of VA hospital buildings has two components—sensing and analysis. The sensing component includes accelerometers, digitizers, servers and all other necessary hardware to measure the response of the building, record the data, and transmit the data to an onsite server in real-time. The number of the accelerometers deployed in each building varies depending on the floor area, the number of stories and the number of the blocks (or wings) the building has. For instance, the main hospital building at the VA medical center in San Diego, California will have a seismic array of 60 accelerometers (see Fig. 2).

The force-balanced accelerometers used are primarily designed for structural engineering applications, and can measure acceleration up to 4 g. Having an adjustable full-scale recording range of ± 0.25 to ± 4 g makes these sensors also suitable to measure low-intensity ambient noise. The accelerometers are wired to a 24-bit IP-based digitizer located in the building. The digitizer works both in continuous recording mode and event-triggered mode. Each hospital building is instrumented in a similar way: The accelerometers are permanently deployed at the locations where the maximum response is expected, mostly the floor edges of the buildings. Every floor in each building has at least three accelerometers oriented horizontally in two orthogonal directions to detect building motion along the reference east-west and north-south directions. Floor rotation around the vertical axis can be computed from the recordings of the two

accelerometers located at different points and oriented in the same direction. Each building also has a tri-axial accelerometer located on the ground (or basement) floor, which provides the base motion in three orthogonal directions. Additionally, some buildings have multiple accelerometers oriented in the vertical direction to determine the building's rocking motions (see Fig. 2). The instrumentation within the hospital buildings is aimed to record floor accelerations, and to compute relative displacement between adjacent floors, as well as overall building roof displacement, floor torsion, building rocking, travel time of transmitted seismic waves between consecutive floors, and the building's modal parameters (vibration periods, mode shapes and modal damping values). More details about the hospital buildings and their instrumentation can be found in Kalkan et al^{5,6,7}.

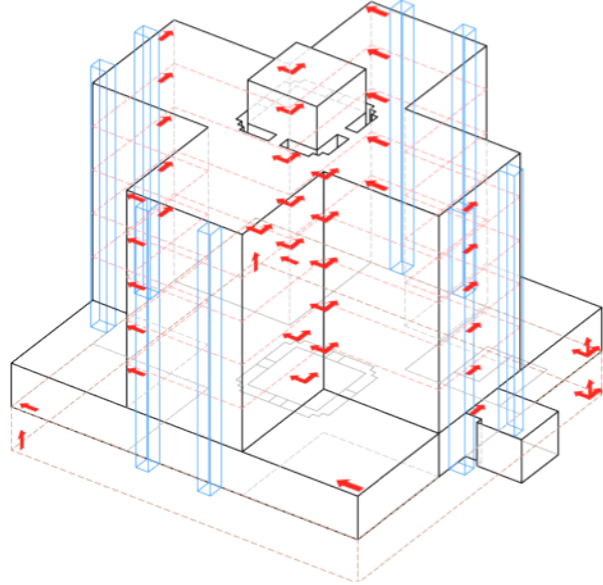


Figure 2. San Diego VA hospital building (left) and its instrumentation diagram (right). Red arrows in the schematic diagram show the locations and indicate the directional sensitivity of the seismic sensors from the basement through the building's seven stories to the roof. The triaxial sensor on the ground floor (at lower right) monitors the input motions in three orthogonal directions.

The analysis component of the system consists of several data processing modules integrated into a software package called “Earthworm”, (Johnson et al.⁸), which is an open source waveform and automated earthquake data processing software. Four separate algorithms are adopted and implemented here to detect and locate probable damage zones in the buildings. These algorithms compute change in modal frequencies and mode shapes of the structure, and track exceedance of design base shear capacity and inter-story drift ratios for various performance levels. Each algorithm is implemented into a separate module. In addition to these damage detection modules, several other modules help data flow through the monitoring system, archive the data, and perform other intermediate data processing. The modules use a set of configuration files, where computational parameters and settings of the data acquisition and firmware can be configured. Further details of the monitoring system are described in Ulusoy et al⁹. The SHM and damage detection system developed for the VA hospital buildings is schematically shown in Figure 3. A USGS open file report fully describing this system is currently underdevelopment.

3. VALIDATION & VERIFICATION

Numerous algorithms have been developed to detect and locate damage using vibration measurements over the past three decades²¹. Most of them were validated analytically without experimental testing. In analytical validations, various damage scenarios are generated using a computer model of a single structural member or a very simple structural system. The validation based on the analytical model solely is not sufficient because uncertainties in modeling and measurement are overly simplified or totally ignored. Thus, experimental validation and if possible, validation of algorithms using field measurements collected from actual structures during severe earthquakes are essential. Data obtained during damaging earthquakes is very limited to a few instrumented buildings, which were not fully instrumented at the time of damaging events recorded (e.g., Imperial County Service Building and North Hollywood

Hotel in Southern California). Thus, experimental data from a series of shake table tests are used here to evaluate three different damage detection algorithms.

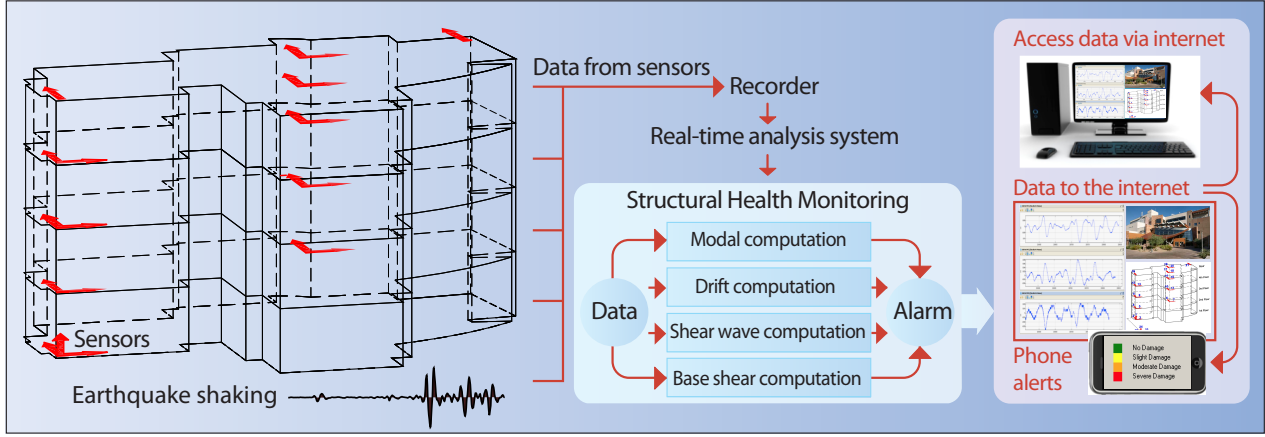


Figure 3. Flow chart showing the functioning of a real-time earthquake monitoring system for instrumented buildings. The system provides important information on the structural health of the building. After a significant earthquake, its near real-time data analysis capabilities help to rapidly assess building safety.

4. SHAKE-TABLE EXPERIMENTS

4.1 Description and Instrumentation of Test Structure

A slice (that is, a cut to mimic a typical vertical configuration) of a full-scale 7-story building was tested under four different earthquake excitations (Fig. 4). The tests took place on a high-performance outdoor shake table at the University of California, San Diego. The objective of the test program was to verify the seismic response of reinforced concrete wall systems designed for lateral forces obtained from a displacement-based design methodology¹⁰.

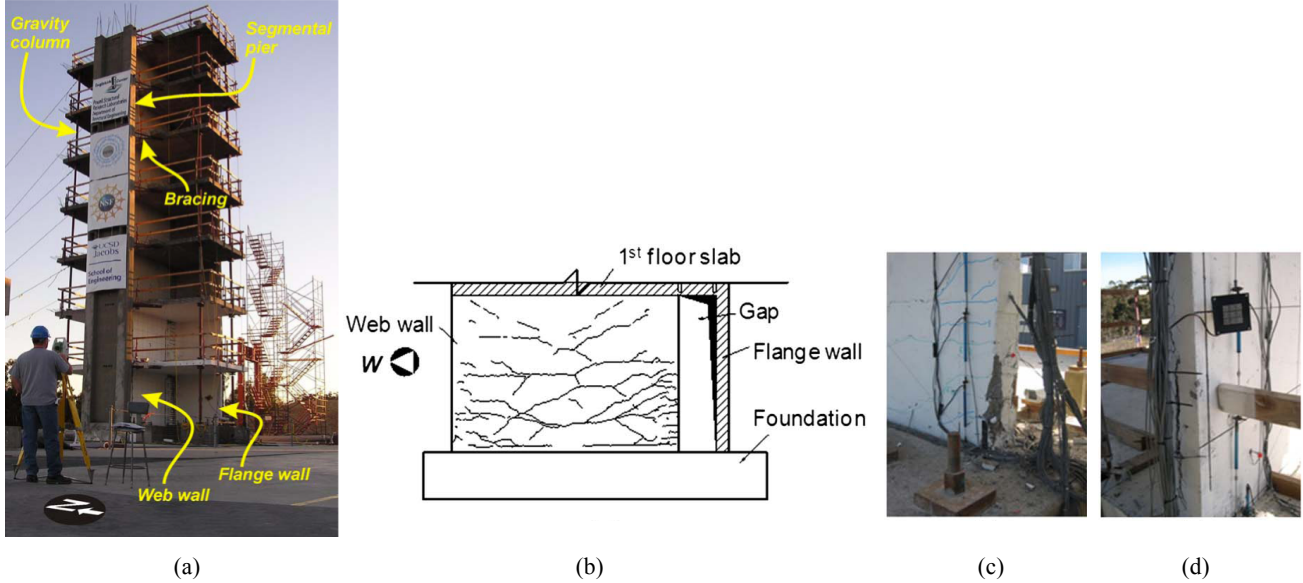


Figure 4. (a) Full-scale test structure; observed damage of web wall after test EQ4; (b) south side view of web wall—Level 1; (c) west bottom end of web wall at Level 1; (d) west bottom end of web wall above first-floor slab (adapted from [11, 20]).

The test structure has the following members: Load bearing web wall is the main member of the structure to be tested. The web wall has rectangular section of 144 inches by 8 inches. The wall provides the significant portion of the lateral stiffness of the structure in the reference east-west direction, which is the shaking direction. Each floor has a rectangular

slab with dimensions of 320 inches by 144 inches. The slab is supported by the web wall and four steel tube columns located near the corners of the slab. A flange wall and a precast wall provide torsional and lateral stiffness to the structures in the reference north-south direction. These two walls are connected to the slab at each floor level with slotted and steel brace connections. The transverse walls are to maintain the stability of the entire structure during shake table tests. The total height of the structure is 756 inches and the total weight is 550 kips. Further details of the test structure and its reinforcement are described in Panagiotou et al¹¹. The test structure, its surrounding soil, and the shake table were instrumented with a total of 139 accelerometers, 88 displacement transducers, 314 strain gages, and 23 pressure transducers. Lateral response of the structure is measured at each floor level by three accelerometers in the reference east-west direction. In addition, a sensor is mounted on the web wall to measure the response at the mid-height of each story. Two accelerometers oriented in the reference north-south direction are placed at each floor level to measure corresponding motion. Another two accelerometers oriented vertically are placed at each floor level to measure vertical motions. The measured data are sampled at a rate of 240 samples per second.

4.2 Test Procedure

The test structure was subjected to a series of earthquake and white noise excitations in the reference east-west direction. The earthquake excitations were selected from the actual ground motions from the 1971 San Fernando and the 1994 Northridge earthquakes. The amplitude of earthquake excitations increases while the tests proceed. The objective of the earthquake excitation tests is to gradually inflict damage into the structure. The first earthquake is a low intensity ground motion with a peak acceleration of 0.15g. The second and third earthquakes are medium intensity ground motions with peak accelerations of 0.27g and 0.34g, respectively. The spectral accelerations of these earthquakes are above the site response spectra for 50% probability of exceedance in 50 years in the frequency range of interest. The fourth earthquake is a high intensity ground motion with a peak acceleration of 0.91g, which is slightly above the site response spectra for 10% probability of exceedance in 50 years.

The earthquake excitation tests are aimed to be destructive, therefore a certain degree of nonlinear-inelastic response is expected during these tests, while the white noise tests are aimed to be nondestructive. It is a fairly valid assumption that the test structure has linear-elastic response under the structure's current condition during white noise tests. The assumption of linear-elastic response is critical to the accuracy of the analysis results as many parameter identification procedures work for linear-elastic systems. In addition, the maximum amplitude of the white noise does not vary much during these tests, which minimizes the effect of amplitude on the parameters identified. Therefore, the white noise data can be used more conveniently to determine the vibration characteristics of the test structure after each earthquake excitation test. Before and after each earthquake excitation, the test structure was subjected to low-intensity white noise shaking. The objective of these white noise tests was to determine the damage state after each earthquake excitation test. The power of these excitations is quantified by the root mean square of 0.02g, 0.03g, and 0.05g. The frequency range of the white noise excitations is 0.5-25Hz. In between two earthquake excitation tests, ambient response of the structure was also measured and recorded. The sequence of the test procedure is summarized in Table 1.

Table 1. Summary of the shake table tests

Test No	Description
1	2%, 3% g RMS white noise sequence test, and ambient vibration
2	Low intensity earthquake: EQ1
3	2%, 3%, 5% g RMS white noise sequence test, and ambient vibration
4	The first medium intensity earthquake: EQ2
5	2%, 3%, 5% g RMS white noise sequence test, and ambient vibration
6	The second medium intensity earthquake: EQ3
7	2%, 3%, 5% g RMS white noise sequence test, and ambient vibration
8	High intensity earthquake: EQ4
9	2%, 3%, 5% g RMS white noise sequence test, and ambient vibration

5. TEST RESULTS AND ANALYSES

The response data measured by fifteen accelerometers mounted on the web wall at each floor level and at mid-height of each story are analyzed to test the damage detection algorithms. The natural frequencies and mode shapes are estimated from the white noise test data before and after each earthquake excitation test. The white noise test data are also utilized to estimate shear-wave travel time from the base through the roof of the structure. The average drift ratios are computed based on data from four earthquake excitation tests.

5.1 Change in Modal Frequencies and Mode Shapes

A paper by Salawu¹² reviews a number of methods using changes in frequencies to detect damage. To track the frequency change during the tests and use it for damage detection, the modal parameters are extracted from the response data by means of modal analysis and system identification. The response of this particular test structure is similar to a cantilever beam, and the first mode dominates the total response. Nevertheless, the first three vibration modes of the test structure are identified from the first white noise test data. These identified modes are associated with the intact (undamaged) structure and provide a set of baseline values for comparison. After each earthquake excitation test, the mode identification procedure is repeated using the subsequent white noise data collected right after the test. The modal frequencies are normalized by the baseline values for ease of comparison. The identified frequencies are shown in Table 2. As the test structure progressively suffers damage, a gradual decrease in the first three modal frequencies after each earthquake excitation test can be observed from the estimated frequency values. Analysis results suggest that even the first earthquake excitation with a peak acceleration of 0.15g results in a 9% reduction in the first modal frequency. A possible explanation for this is that cracks develop in the concrete during the test, thus the effective section stiffness decreases, and the structure becomes less stiff. After the test micro cracks were observed and marked on the web wall at the first story; the strain gage envelope also confirms that the concrete cracking strain is exceeded during the test¹¹.

The test structure sustains damage due to the second and third earthquake excitations. Minor cracks on the web wall were observed. A decrease of 26% and 34% in the first modal frequency can be seen from the frequency estimation results after the second and the third earthquake excitations, respectively. The effective stiffness further decreases due to new crack developments in a wider area and due to the growing of the existing cracks. This result is also consistent with the visual inspections (see Fig. 4b,c,d) and the strain gage data collected right after the first and second earthquake excitation test. The decrease in the second and third modal frequencies is lower than that in the first modal frequency after these earthquakes. A significant drop of 51% in the first modal frequency is observed after the fourth earthquake excitation test. The drops in the second and third modal frequencies computed are also significant. During the test, limited spalling of the concrete cover at the base of the web wall and large split crack at the west lap-splice at the base of the second floor level were reported after the visual inspections. Strain gage measurements show that the steel tensile strain exceeds the yield strain at the first and second stories during the test.

Table 2. First three fundamental modal frequencies of the test structure identified from the white noise tests data

White Noise Test	Mode-1		Mode-2		Mode-3	
	Estimated Frequency (Hz)	Normalized Frequency	Estimated Frequency (Hz)	Normalized Frequency	Estimated Frequency (Hz)	Normalized Frequency
1	1.72	1.00	10.17	1.00	23.57	1.00
3	1.56	0.91	9.84	0.97	24.13	1.02
5	1.27	0.74	8.66	0.85	23.43	0.99
7	1.14	0.66	7.91	0.77	21.11	0.90
9	0.85	0.49	5.10	0.50	15.26	0.65

The modal analysis results suggest that the natural frequencies of the test structure are sensitive to damage; therefore the change in natural frequencies may be used as an indicator to detect possible damage. Even minor cracks observed after the second earthquake with a peak acceleration of 0.27g causes a 26% decrease in the first modal frequency. The frequency is a single global parameter that depends on the mass, stiffness, and damping properties distributed over the

structure, and does not provide any information regarding location of the damage. On the other hand, the mode shapes represent the deflection patterns of the structure at resonance frequencies, and each component of the mode shape vector carries information corresponding to the location where a motion sensor is placed. The mode shapes were estimated from the white noise tests after each earthquake excitation test. Figure 5 shows the first three mode shapes of the structure together with the mode shapes of the damaged structure after each earthquake excitation test.

To measure the correlation between two sets of mode shape vectors, the modal assurance criterion (MAC) is used. The mode shapes estimated after each earthquake excitation test are compared to those estimated from the first white noise test. The MAC was devised to provide a single numerical value that indicates the correlation between mode shapes. When two structures' mode shapes are fully correlated, the corresponding MAC has a value of 1, whereas fully uncorrelated mode shapes are indicated by a MAC value 0. The formulation of MAC is as follows:

$$MAC_{cdr} = \frac{\left| \sum_{q=1}^{N_o} \phi_{cqr} \phi_{dqr}^* \right|^2}{\sum_{q=1}^{N_o} \phi_{cqr} \phi_{cqr}^* \sum_{q=1}^{N_o} \phi_{dqr} \phi_{dqr}^*} \quad (1)$$

where ϕ_{cqr} is the modal coefficient for degree-of-freedom q , mode r and N_o is number of degree of freedom. Based on Eq. (1), the MAC values computed after each earthquake excitation test are given in Table 3. The MAC values clearly show that the change in the mode shapes is not as significant as the change in the frequencies as the test structure gradually sustains damage after each earthquake excitation test. In other words, change in mode shapes are influenced by major damage. Based on the MAC values, one can claim that the first three mode shapes remain unchanged after the first three earthquake excitation tests, which cause minor damage to the structure. Only, the second and the third mode shapes noticeably change after the fourth earthquake that causes severe damage to the structure.

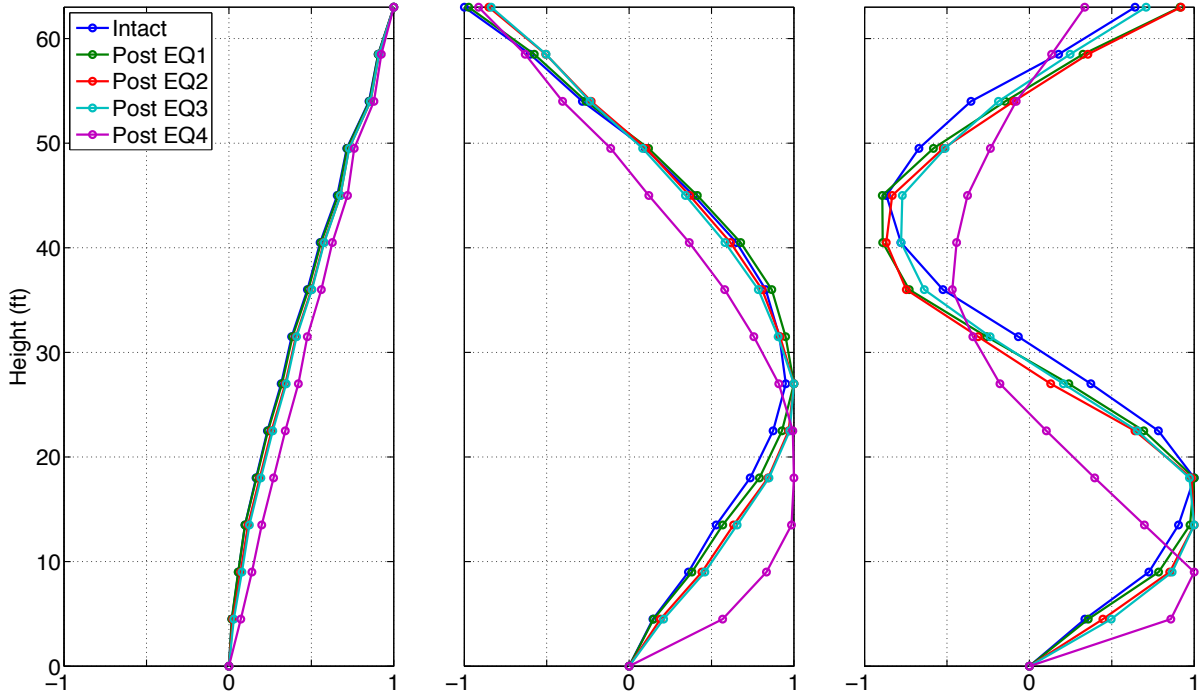


Figure 5. Normalized mode shapes for first three fundamental modes of the test structure computed using white noise test data.

Damage results in decrease in stiffness, which in turn results in stress redistribution and change in section forces. Another parameter that can be derived from the mode shapes is the curvature, which is directly related to section bending moment¹³. The curvature at the intermediate points along the height of the test structure is derived from the first mode shapes using the finite difference approximation. Then, the relative change in the curvature along the height of the

test structure is computed after each earthquake excitation test. Unlike the mode shapes, the analysis results show that the change in mode shape curvature is more sensitive to damage, and it successfully locates the damage zones in the structure. Figure 6 shows the relative changes in the mode shape curvature concentrated mainly along the height of the first and second stories. The relative changes in the damaged area consistently grow with the intensity of earthquake shaking and extent of the damage observed after each earthquake excitation test. These results are verified with the visual damage inspections.

Table 3. MAC values computed from the two sets of the mode shape vectors of the intact structure and damaged structure after each earthquake excitation test.

	Mode 1	Mode 2	Mode 3
Post EQ1	1.000	0.999	0.961
Post EQ2	0.999	0.988	0.936
Post EQ3	0.999	0.984	0.964
Post EQ4	0.989	0.861	0.606

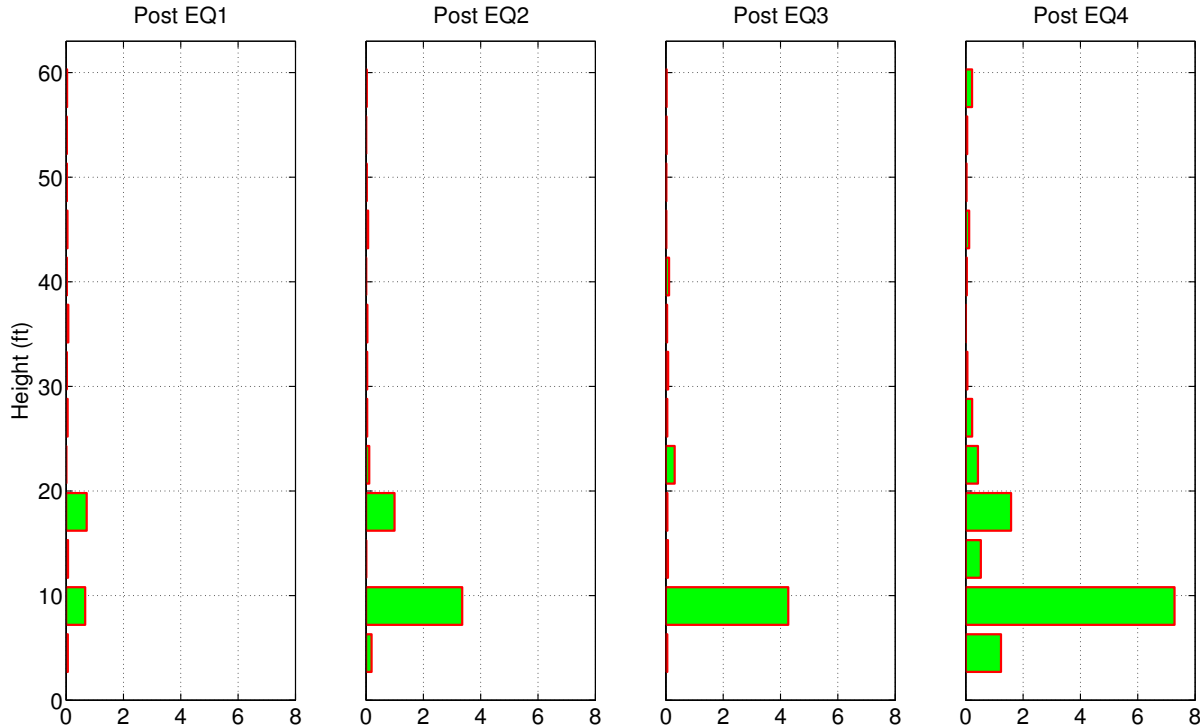


Figure 6. Relative changes with respect to pre-test (intact) condition in first fundamental mode shape curvatures computed after each earthquake excitation.

5.2 Change in Shear-wave Travel Time

Analogous to shear-wave propagation in soil with multiple layers of varying medium parameters, a one-dimensional shear-wave propagation model can be used to analyze the response of a multi-story building¹⁴. By deconvolving the waveforms at different locations, the wave travel time and an average shear-wave velocity can be obtained. The wave travel time in each story depends on the stiffness and mass density of the story. Therefore, tracking the change in wave travel time can be used to detect the change in stiffness that may indicate damage^{15,16}. In this study, the white noise test

data after each earthquake are utilized to compute shear-wave travel time through the height of the structure. In theory, the arrival time of the shear-wave that travels upward and downward through the test structure can be estimated from the response recorded at the basement floor and the top floor in two ways: The top floor response can be deconvolved by the basement floor response, or the basement floor response can be deconvolved by the top floor response. The waveforms deconvolved by the basement floor are complicated, therefore the arrival time of the shear-wave is estimated by deconvolving the response measured at the lower floor levels by the top floor response. A moving time window of 12.5 seconds is used to compute the wave travel time (see Fig. 7a). The analysis results prove that white noise response data yield more consistent results than the earthquake response data. The travel time obtained from each window is almost the same as those obtained from the other windows. Figure 7b shows a snapshot of the deconvolved waveforms where the upward and downward travelling shear-waves are evident.

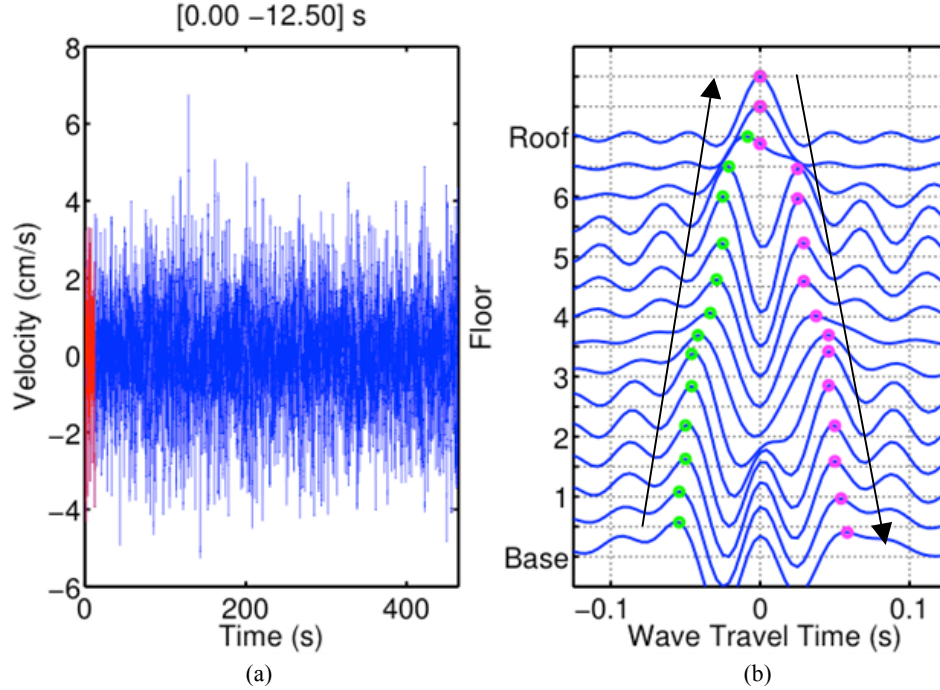


Figure 7. (a) Time interval (shown with red color) is shown for deconvolution of waves and for peak picking (as marked in panel “b” with green and magenta circles); (b) Deconvolved waves are shown; upward and downward travel times are indicated with arrows.

Figure 8 shows the shear-wave travel time obtained after each earthquake excitation test. The figure shows that wave travel time for the first two stories is larger after each test. This indicates a reduction in stiffness of the first two stories. This result is consistent with the visual inspection after each earthquake excitation test. The effective stiffness of the first two stories is reduced due to the cracks and concrete spalling.

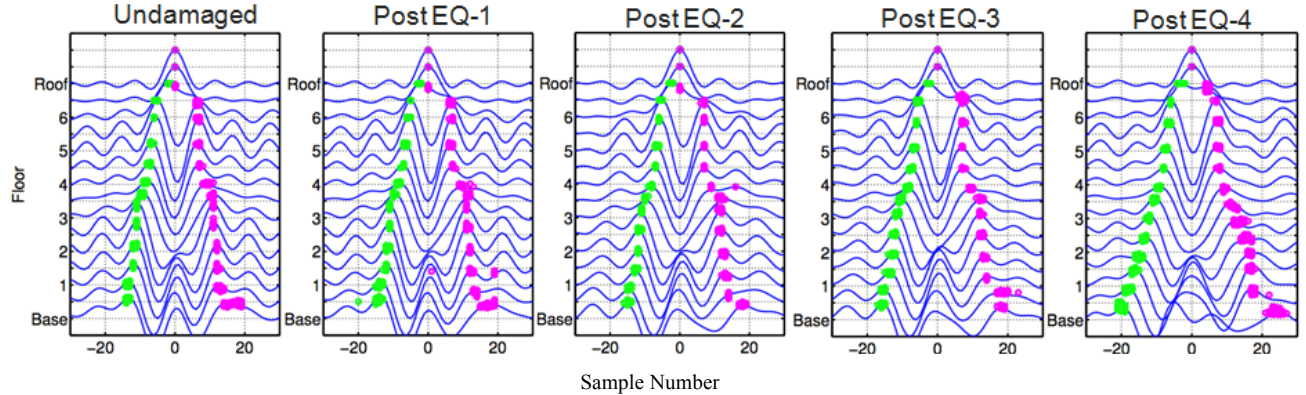


Figure 8. Deconvolved waves of undamaged and post earthquake in 7-story RC building test specimen. It can clearly be seen that damage in the building affects the wave travel times. The arrival time of the waves from basement to top was below 20 time steps (approx. 10-15 time steps) in undamaged condition. However, after damage appears in the building the wave travel times started to increase. As EQ4 caused the most severe damage in the building, an increase in the damage level results in an increase in the wave travel times.

5.3 Inter-story Drift Ratio

The inter-story drift ratio is a commonly used engineering demand parameter in the design of new buildings and in the performance evaluation and rehabilitation of existing buildings. FEMA 450¹⁷ defines four performance levels of buildings under earthquake loads: (1) Operational, (2) Immediate occupancy, (3) Life safety, and (4) Collapse prevention. In FEMA 450¹⁷ and ASCE 41-6¹⁸ guidelines these performance levels are linked to drift values for different types of structures. The drift ratios associated with three performance levels for concrete and steel members are summarized in Table 4. With the drift limit ratios defined for three different performance levels, the ability to derive the drift ratios from measured acceleration data allows one to rapidly assess the damage state of building structures after an earthquake.

Table 4. The drift limits and associated performance levels for the vertical member adapted from ASCE 41-06 guidelines¹⁸

Vertical Elements	Structural Performance Levels		
	Immediate Occupancy	Life Safety	Collapse Prevention
Concrete Frames	1% Transient Negligible Permanent	2% Transient 1% Permanent	4% Transient or Permanent
Steel Moment Frames	0.7 % Transient Negligible Permanent	2.5 % Transient 1% Permanent	5 % Transient or Permanent
Concrete Walls	0.5% Transient Negligible Permanent	1% Transient 0.5% Permanent	2% Transient or Permanent

To test the feasibility of the use of inter-story drift ratio for damage detection, the earthquake excitation test data are analyzed. After baseline correction and double integration, the displacement for each story is derived from the measured acceleration data. The inter-story drift ratio can be computed from relative horizontal displacement of each story for multi-story buildings with moment frame system based on the premise that the lateral deformation of this kind of building is analogous to shear deformation. However, this premise is not correct for the test structure as the lateral deformation is dominated by bending (flexural). Figure 9 illustrates how to compute the relative rotation of a cantilever

beam from the horizontal displacement. Instead of inter-story drift ratio, an average drift ratio for the entire structure is derived from the relative roof displacement.

Figure 10 shows the average drift ratio due to the four earthquake excitation tests. The peak average drift ratio due to the first earthquake excitation test is 0.24%, which is lower than the drift limit for immediate occupancy performance level for a concrete wall building. Peak average drift ratios of 0.62% and 0.68% are computed during the second and third earthquake excitation tests, respectively. These drift ratios are slightly higher than the drift ratio specified for the *immediate occupancy* performance level. This implies that “the building” cannot be occupied immediately after these earthquakes but may be reoccupied after necessary repairs and rehabilitations. A peak average drift ratio of 1.37% is computed during the fourth earthquake excitation test, which is higher than the drift limit specified for the *life safety* performance level. The visual damage inspection shows that the test structure suffered severe damage during the fourth earthquake but did not collapse and the web wall was still functional. A comparison of the computed drift ratios to the drift limits specified in the ASCE 41-06 suggest that “the building” can be occupied after the first earthquake. “The building” cannot be occupied after the second and third earthquake. The average drift limit computed during the fourth earthquake is higher than that of *life safety* performance level, which suggests that “the building” may pose life safety hazard to its occupants.

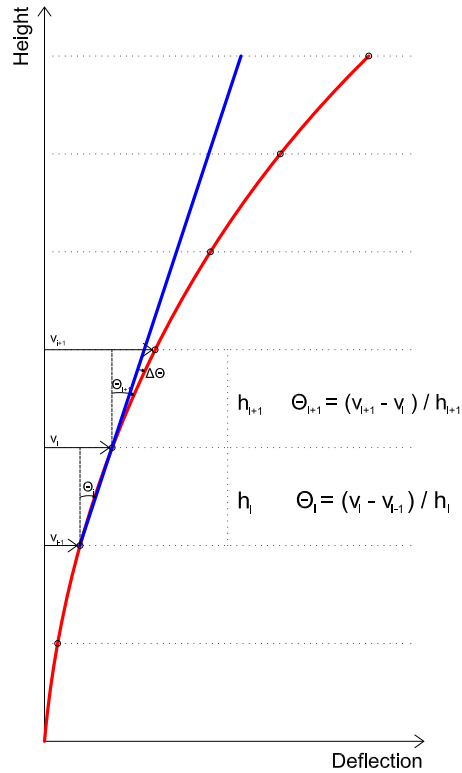


Figure 9. Relative rotation of a cantilever beam from the horizontal displacement.

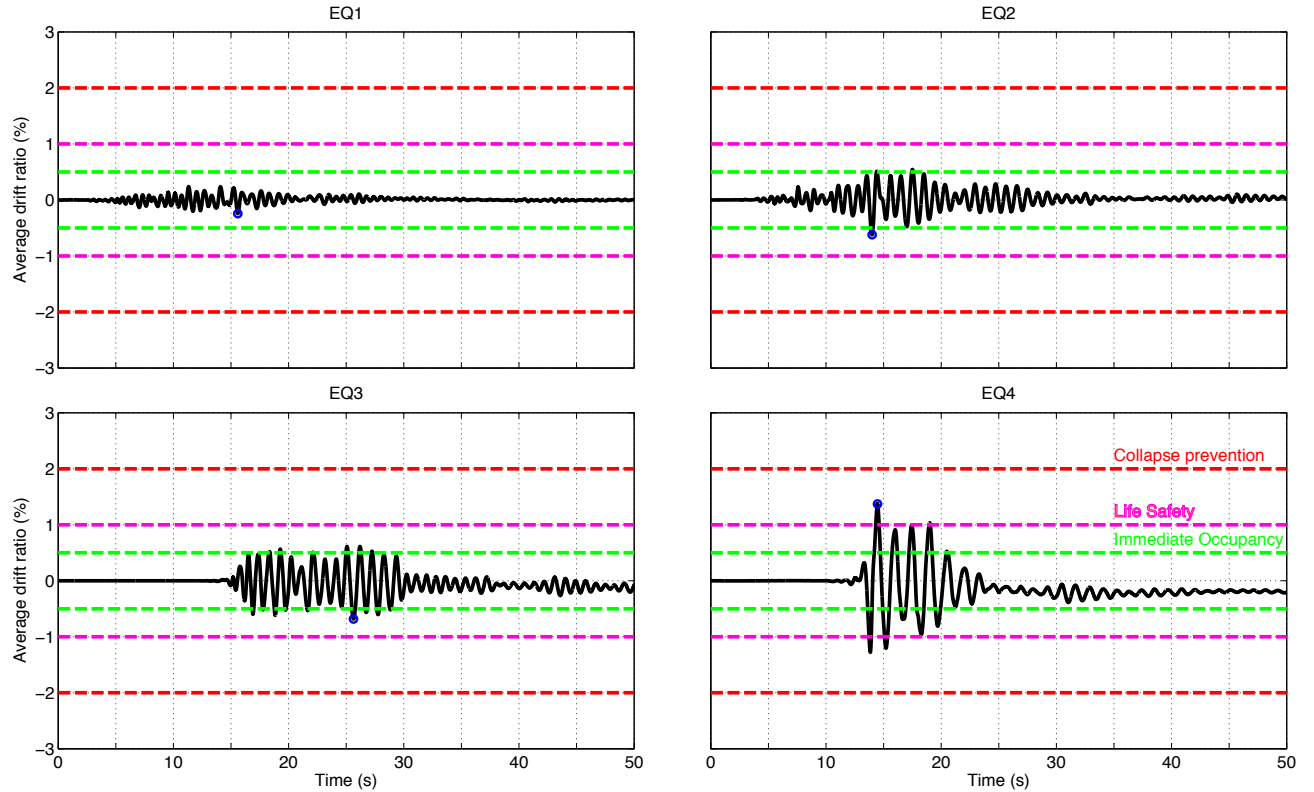


Figure 10. Average drift ratio variation (in percent) during four earthquake excitations (EQ1 thru EQ4); performance levels according to the ASCE 41-06 guidelines are indicated with horizontal dashed lines; peak values of average drift are indicated by blue circles.

6. SUMMARY & CONCLUSIONS

The initial validation and verification of an advanced structural health monitoring (SHM) system, currently under development for Veterans Affairs' hospital buildings across the U.S., are presented. This (SHM) system utilizes four different damage detection algorithms to compute changes in shear-wave travel time, modal parameters, design base shear force, and inter-story drift ratios using the measured vibration data only from the instrumented building without requiring any complex models (e.g., finite element model). In this study, three out of four algorithms are validated against the experimental vibration data obtained from a full-scale structure tested on the University of California, San Diego shake-table. The test structure represents a particular type of shear-wall dominant reinforced concrete building¹⁹. With its full-scale test procedure, and extensive instrumentation, these shake table tests provided a comprehensive dataset for testing the damage detection algorithms in a realistic way. The conclusions drawn from this validation study are as follows:

1. Comparison of analytical results with the experimental data shows that qualitative damage descriptions match well the quantitative results obtained by the three damage detection algorithms.
2. Comparison of the structure's fundamental frequencies identified from the white noise test data before and after each earthquake excitation test demonstrates that the observed frequency shifts are consistent with actual damage conditions of the structure. For practical application, one can replace white noise measurements with ambient noise measurements. It is also known that a significant variation in frequencies that might be misinterpreted as damage can be observed during different earthquakes²². Such variation may result from the amplitude variation of shaking, nonlinearity, soil-structure interaction, and other factors (e.g., contribution of non-structural components into a structure's stiffness and strength). Distinguishing the frequency shifts associated with such effects from those due to actual damage conditions is not an easy task; therefore, using the frequency shifts for damage detection during an earthquake is likely to be the least reliable method.

3. The mode shape curvatures of the damaged structure after each earthquake excitation test are compared with the mode shape curvatures of the intact structure to detect and locate possible damage zone(s). For this particular test structure, the mode shape curvatures successfully identified the damage zones in the structure. The analysis results show that the most significant changes in mode shape curvature are at the first two stories, consistent with visual damage inspections.
4. Another approach to locate damage is to use waveform deconvolution that leads to shear-wave travel time through the test structure. The waveforms deconvolved by the top floor response clearly show gradual elongations in the travel time in the first two stories after each earthquake excitation test. This approach seems promising for shear-wall dominant buildings where the response can be represented with one-dimensional wave propagation. The use of this approach for damage detection in short-wide moment-frame buildings remains to be tested and verified.
5. The use of inter-story drift ratio is the most practical approach for damage detection and localization in multi-story buildings. Since drift computation does not require any underlying physical model, it can be used for all kinds of building structures. The major concerns in implementing the inter-story drift ratio in damage detection are that the accuracy of the drift computation plays a critical role for reliable damage detection decision, and the threshold limits given in various design and rehabilitation codes to define damage state are generic values. For the test structure considered in this study, the average drift ratios are computed from the earthquake response, and the corresponding damage states are identified in accordance with the drift ratio limits specified in the ASCE 41-06¹⁸ guidelines. The damage states of the test structure concluded from the computed drift ratios are in a reasonably good agreement with the visual inspections after each test.

ACKNOWLEDGMENTS & RESOURCES

We would like to thank Prof. Babak Moaveni for providing us the University of California, San Diego experimental shake table test data. We also thank Drs. Kishor Jaiswal, Reza Baghaei and Keith Knudsen for their review and constructive comments. The U.S. Department of the Veterans Affairs has provided funding for this study. Details of the seismic instrumentation project for Veterans Affairs hospital buildings, and numerous publications of this project can be found at <http://earthquake.usgs.gov/monitoring/buildings/va.php>.

REFERENCES

- [1] Friswell, M. I., "Inverse Problems in Structural Dynamics", Proceedings of the 2th International Conference on Multidisciplinary Design Optimization and Applications", Gijon, Spain (2008).
- [2] Carden, E. P. and Fanning, P., "Vibration based condition monitoring: A review", Structural Health Monitoring (3)4, 355–377 (2004).
- [3] Doebling, S. W., Farrar, C. R., Prime, M. B. and Shevitz, D. W., "Damage identification and health monitoring of structural and mechanical systems from changes in their vibration characteristics: a literature review", Technical Report LA-13070-MS, Los Alamos National Laboratory, Los Alamos, NM, (1996).
- [4] Sohn, H., Farrar, C. R., Hemez, F. M., Shunk, D. D., Stinemates, D. W. and Nadler, B. D., "A review of structural health monitoring literature: 1996–2001", Technical Report: LA-13976-MS, Los Alamos National Laboratory, Los Alamos, NM, (2003).
- [5] Kalkan, E., Banga, K., Ulusoy, H. S., Fletcher, J. P. B., Leith, W. S., Reza, S. and Cheng, T., "Advanced earthquake monitoring system for U.S. Department of Veterans Affairs medical buildings–instrumentation", U.S. Geological Survey Open–File Report: 2012–1241, (2012); available online at <http://pubs.usgs.gov/of/2012/1241/>.
- [6] Kalkan, E., Banga, K., Ulusoy, H. S., Fletcher, J. P. B., Leith, W. S. and Blair, J. L., "Helping safeguard Veterans Affairs' hospital buildings by advanced earthquake monitoring", U.S. Geological Survey Fact Sheet 2012–3094, (2012); available online at <http://pubs.usgs.gov/fs/2012/3094/>.
- [7] Kalkan, E., Fletcher, J. P. B., Leith, W. S., McCarthy, J. and Banga, K. (2012b), "Real-time seismic monitoring of instrumented hospital buildings", U.S. Geological Survey Fact Sheet 2012–3028, (2012); available online at <http://pubs.usgs.gov/fs/2012/3028/>.

- [8] Johnson, C. E., Bittenbinder, A., Bogaert, B., Dietz, L. and Kohler, W., "Earthworm: A flexible approach to seismic network processing", IRIS Newsletter 14(2), 1–4, (1995).
- [9] Ulusoy, H. S., Kalkan, E., Fletcher, J. P. B., Friberg, P., Leith, W. K., and Banga, K., "Design and implementation of a structural health monitoring and alerting system for hospital buildings in the United States", Proceedings of the 15th World Conference on Earthquake Engineering, Lisbon, Portugal (2012); available online at http://nsmp.wr.usgs.gov/ekalkan/PDFs/A87_Ulusoy_et_al.pdf.
- [10] Panagiotou, M., Restrepo, J. I. and Conte, J. P., "Shake-Table Test of 7-Story Building Slice. Phase I: Rectangular Wall", Journal of Structural Engineering–ASCE 137(6), 691–704, (2011).
- [11] Panagiotou, M., Restrepo, J. I. and Conte, J. P., "Shake-Table Test of 7-Story Building Slice. Phase I: Rectangular Wall Section", University of California, San Diego. Technical Report: SSRP-07-07, (2007).
- [12] Salawu, A. S., "Detection of structural damage through changes in frequency: a review", Engineering Structures 19(9), 718–723, (1997).
- [13] Pandey, A. K., Biswas, M. and Samman, M. M., "Damage Detection from changes in curvature mode shapes", Journal of Sound and Vibration 145(2), 321–332, (1991).
- [14] Snieder, R. and Safak, E., "Extracting the Building Response Using Seismic Interferometry: Theory and Application to the Millikan Library in Pasadena, California", Bulletin of the Seismological Society of America 96(2), 586–598, (2006).
- [15] Todorovska, M. I. and Trifunac, M. D., "Impulse response analysis of the Van Nuys 7-story hotel during 11 earthquakes and earthquake damage detection", Structural Control and Health Monitoring 15(1), 90–116, (2008).
- [16] Todorovska, M. I. and Trifunac, M. D., "Earthquake damage detection in the Imperial County Services Building–I: The data and time–frequency analysis", Soil Dynamics and Earthquake Engineering 27(6), 564–576, (2007).
- [17] Federal Emergency Management Agency, "FEMA 450– NEHRP Recommended Provisions and Commentary for Seismic Regulations for New Buildings and Other Structures", Federal Emergency Management Agency, Washington, DC, (2003).
- [18] American Society of Civil Engineers, "Seismic Rehabilitation of Existing Buildings", Report No: 41–6, American Society of Civil Engineers, Reston, VA, (2007).
- [19] Balkaya, C. and Kalkan, E., "Seismic Vulnerability, Behavior and Design of Tunnel Form Buildings", Engineering Structures 26(14), 2081-2099, (2004); available online at http://nsmp.wr.usgs.gov/ekalkan/PDFs/A26_Balkaya_Kalkan.pdf.
- [20] Moaveni, B., He, X., Conte, J. P., Restrepo, J. I., and Panagiotou, M., "System identification study of a seven-story full-scale building slice tested on the UCSD-NEES shake table", Journal of Structural Engineering, ASCE 137(6), 705–717, (2011).
- [21] Catbas F. N., Kijewski-Correa, T. and Aktan A. E., "Structural Identification of Constructed Facilities", State-of-the-Art Report by American Society of Civil Engineers / Structural Engineering Institute (ASCE/SEI), 236 p., (2011).
- [22] Ulusoy, H. S., Feng, M. Q. and Fanning, P. J., "System identification of a building from multiple seismic records", Earthquake Engineering & Structural Dynamics 40(6), 661–674, (2011).